Coupling mechanisms in double sandbar systems. Part 1: Patterns and physical explanation

Bruno Castelle[1,2]*, B. G. Ruessink[3], Philippe Bonneton[1,2], Vincent Marieu[1,2], Nicolas Bruneau[1,2] and Timothy D. Price[3]
[1] CNRS, UMR EPOC 5805, Talence, F-33405, France
[2] Université de Bordeaux, UMR EPOC 5805, Talence, F-33405, France
[3] Institute for Marine and Atmospheric Research, Department of Physical Geography, Utrecht University, The Netherlands

*Correspondence to: Bruno Castelle, CNRS, UMR EPOC 5805, Talence F-33405, France. E-mail: b.castelle@epoc.u-bordeaux1.fr

ESPL

Earth Surface Processes and Landforms

ABSTRACT: Crescentic sandbars and rip channels along wave-dominated sandy beaches are relevant to understand localized beach and dune erosion during storms. In recent years, a paradigm shift from hydrodynamic template models to self-organization mechanisms occurred to explain the formation of these rhythmic features. In double sandbar systems, both the inner- and outer-bar rip channels and crescentic planshapes are now believed to be free instabilities of the nearshore system arising through self-organization mechanisms alone. However, the occasional occurrence of one or two inner-bar rip channels within one outer-bar crescent suggests a forced, morphologically coupled origin. Here we use a nonlinear morphodynamic model to show that along-shore variability in outer-bar depth, and the relative importance of wave breaking versus wave focussing by refraction across the outer bar, is crucial to the inner-bar rip channel development. The coupling patterns simulated by our model are similar to those observed in the field. Morphological coupling requires a template in the morphology (outer-bar geometry) which, through the positive feedback between flow, sediment transport and the evolving morphology (that is, self-organization) enforces the development of coupling patterns. We therefore introduce a novel mechanism that blurs the distinction between self-organization and template mechanisms. This mechanism may also be extended to explain the dynamics of other nearshore patterns, such as beach cusps. The impact of this novel mechanism on the alongshore variability of inner-bar rip channels is investigated in the companion paper. Copyright © 2010 John Wiley and Sons, Ltd.

KEYWORDS: self-organization; forcing templates; morphological coupling; coupling patterns; double sandbar system

Introduction

Nearshore patterns along sandy wave-dominated beaches cover a wide and intriguing variety of temporal and spatial variability: ripples (Traykovski *et al.*, 1999; Marieu *et al.*, 2008) and megaripples (Clarke and Wermer, 2004; Gallagher *et al.*, 1998), shoreline undulations ranging from a few (beach cusps, Guza and Inman, 1975; Coco *et al.*, 1999) to hundreds (megacusps, Short, 1999) and thousands (coastline features such as cuspate patterns, Ashton *et al.*, 2001; Ruessink and Jeuken, 2002) of metres and three-dimensional (3D, Short, 1999; Van Enckevort *et al.*, 2004) or alongshore-uniform (Greenwood and Davidson-Arnott, 1979; Short, 1991) surf-zone sandbars. These striking patterns in the nearshore display complex behaviour seemingly at odds with their simplicity and rhythmicity. Their generation and dynamics have puzzled scientists for decades, and debates and unknowns remain within the nearshore community (Coco and Murray, 2007).

Among these morphological features, surfzone sandbars are some of the most intriguing, dynamical and complex patterns. Surfzone sandbar morphology has been studied for a long time (Shepard, 1952). Most of the time, 3D morphological rhythmic or quasi-rhythmic features are observed, which can be viewed as an alongshore sequence of horns (shoals) and bays (cross-shore troughs) alternating shoreward and seaward of a line parallel to the beach (Van Enckevort *et al.*, 2004). These 3D patterns are often part of an accretionary, down-state sequence developing from an alongshore-uniform beach state (Wright and Short, 1984; Ranasinghe *et al.*, 2004) following a storm event. The resulting nearshore patterns are the so-called crescentic sandbars (Van Enckevort *et al.*, 2004; Castelle *et al.*, 2007), also known as lunate bars (Shepard, 1952), and rip channels (Holman *et al.*, 2006; Thornton *et al.*, 2007), also known as transverse or oblique bars and rips morphology (Wright and Short, 1984; MacMahan *et al.*, 2005).

Coco and Murray (2007) reviewed the paradigm shift from template forcings to self-organization mechanisms that occurred in recent years to explain the generation and subsequent nonlinear evolution of 3D surfzone sandbars. A few decades ago, edge waves (i.e. longshore periodic gravity waves trapped to the shoreline by refraction and reflection) appeared as ideal candidates to explain the formation of

alongshore rhythmic patterns such as crescentic sandbars (Bowen and Inman, 1971) and transverse bars (Holman and Bowen, 1982). The cross-shore and alongshore edge-wave patterns are spatially organized structures in the hydrodynamics that were hypothesized to become imprinted on the seabed. Theoretically, in the bottom boundary layer, the second-order drift velocities induced by the standing edge wave are cellular. Assuming that sediment transport takes place mainly close to the bed, there is a potential for a net sediment transport with a horizontal divergence away from nodal lines and toward antinodal lines (Carter et al., 1973), that is, forming the onshore horns of the bar facing the alongshore nodes of the standing edge wave. This hydrodynamic template forcing became widely accepted (Carter, 1988; Komar, 1998; Short, 1999), despite a number of possible objections progressively raised by several authors (Sonu, 1972; Bryan and Bowen, 1997; Bowen, 1997; Holman, 2000; Van Enckevort et al., 2004). Most importantly, the edge-wave theory, which only assumes a passive response of the incipient sediment patterns to the template in the hydrodynamics, is incompatible with the non-linear and open nature of natural nearshore systems (Van Enckevort et al., 2004; Coco and Murray, 2007). In other words, the template forcing theory does not take into account the feedback between hydrodynamics (waves and currents), sediment processes and the evolving morphology.

Only recently, this template forcing theory has been challenged by the development of self-organization models based on this feedback. Linear stability models (Deigaard et al., 1999; Falqués et al., 2000; Damgaard et al., 2002; Calvete et al., 2005, among others), restricted to the initial development (linear regime) of the 3D patterns using a number of simplifying assumptions, have established the role of self-organization mechanisms in the development of crescentic sandbars and transverse bars and rips patterns (Caballeria et al., 2002). Nonlinear morphodynamic models (Damgaard et al., 2002; Reniers et al., 2004; Klein and Schuttelaars, 2006; Castelle et al., 2006; Drønen and Deigaard, 2007; Smit et al., 2008; Garnier et al., 2008, among others) were also used to simulate the formation and subsequent nonlinear evolution of crescentic features. In particular, temporal changes in the wavelength and the amplitude of the 3D patterns, resulting from merging and splitting of individual crescents or rip channels (widely observed in the field, e.g. Van Enckevort et al., 2004), were obtained (Garnier et al., 2008). All these complex and more simple models have established that 3D surfzone sandbars can be formed through self-organization mechanisms alone, and do not require a template in the hydrodynamics.

Double sandbar systems often exhibit reasonably regular outer-bar crescentic patterns and inner-bar transverse bar-rip morphology. Although such double-bar patterns are nowadays believed to be free instabilities of the nearshore system and thus to be formed through self-organization mechanisms, some observations suggest inner-bar variability to be a forced response to outer-bar patterns rather than to be local free instabilities (Figure 1). The striking relationship between inner- and outer-bar patterns can be considered as reminiscent of the more commonly observed relationship between inner-bar patterns and shoreline rhythms (Wright and Short, 1984; Short, 1999; Coco et al., 2005; Thornton et al., 2007). For instance, Sonu (1973) observed a 180° out-of-phase relationship of inner-bar patterns and shoreline rhythms, i.e. an inner-bar bay facing a seaward bulge in the shoreline (Figure 2a). An in-phase relationship can also sometimes be observed (Figure 2b) with an inner-bar horn facing a seaward bulge in the shoreline. On the one hand, in many documented observations of double sandbar systems (Hom-ma and Sonu, 1962; Goldsmith et al., 1982; Bowman and Goldsmith, 1983), no phase coupling has been observed, even when the outer-bar horns are welded to the inner bar. On the other hand, Van Enckevort and Wijnberg (1999) observed inner-bar bays to systemati-
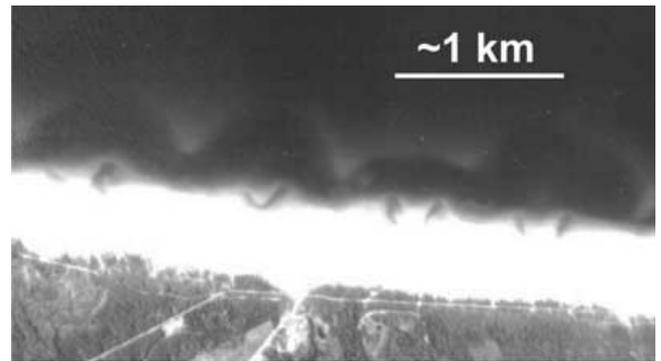
Figure 1. Aerial photograph of a double-barred beach along the Aquitanian Coast revealing the systematic occurrence of two inner-bar rip channels within one outer-bar crescent, suggesting inner-bar variability to be a forced response to outer-bar patterns rather than local free instabilities.
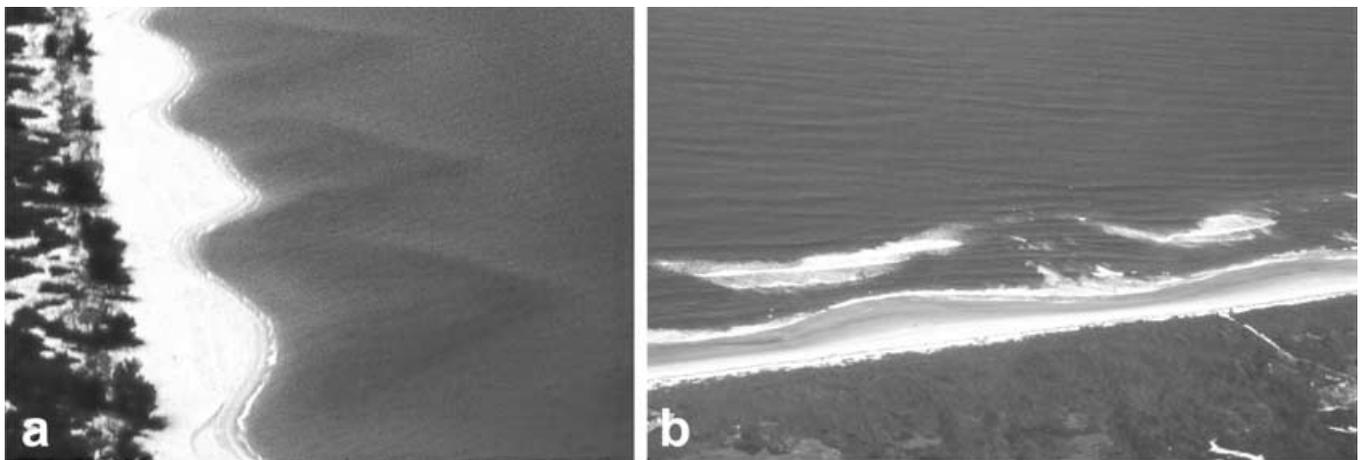
Figure 2. Aerial photographs of a single-barred beach of the New South Wales Coast (Australia) displaying (a) a 180° out-of-phase relationship of inner-bar patterns and shoreline rhythms with inner-bar bays systematically facing a seaward bulge in the shoreline and (b) an in-phase relationship between inner-bar patterns and shoreline rhythms (courtesy of A. D. Short).

cally face outer-bar horns, a situation reminiscent of the commonly observed 180° out-of-phase relationship of inner-bar patterns and shoreline rhythms (Sonu, 1973). Quartel (2009) observed a coupling of the intertidal morphology to the subtidal alongshore variability, with the phase between the two bar variabilities varying from in-phase (0°) to out-of-phase (180°), with gradual phase changes due to different alongshore migration rates of the bars. In addition, Castelle et al. (2007) noted the systematic occurrence of two inner-bar rip channels within one outer-bar crescent, revealing the existence of a possible relationship at half of the outer-bar wavelength. Ruessink et al. (2007) recently examined an eight-week dataset of daily time-exposure video images and showed that, over time, the inner-bar morphology appeared to couple with the crescentic pattern in the outer bar, with the inner-bar morphology developing in response to the increasingly crescentic, onshore-propagating outer bar. This forced morphological response is presumably due to inner-bar wave height variability and associated circulation patterns enforced by the alongshore variability in depth and position of the outer bar (e.g. Castelle and Bonneton, 2004). At this time, however, previous modelling exercises of double sandbar dynamics (Klein and Schuttlelaars, 2006: Drønen and Deigaard, 2007; Smit et al., 2008) did not investigate the potential role of coupling, and the simulation of the observed coupling patterns in double sandbar systems has never been attempted.

The causative mechanisms leading to the apparent coupled and non-coupled behaviour in 3D patterns of double sandbar systems are not well understood. Here we use a nonlinear morphodynamic model (next section) to demonstrate that, as suggested by observations, the variability in mean water depth along the outer bar is crucial to the evolution of inner-bar rip channels and the generation of coupling patterns, with simulated coupling patterns being in agreement with some observations (Results section). In the final section, we discuss the mechanism leading to coupling in double sandbar systems which appears as a novel mechanism that blurs the distinction between self-organization and template mechanisms. This mechanism may also be applied to other nearshore patterns such as beach cusps.

Nonlinear Morphodynamic Model

Model set-up

We used a nonlinear morphodynamic model (Castelle et al., 2006) that couples a spectral wave model, a time- and depth-averaged flow model, an energetic-type sediment transport model, and the bed level continuity equation to compute bed level changes. The spectral wave model SWAN (Booij et al., 1999) is used to compute the wave field and radiation stress components to drive the flow model. The wave field is described with the 2D wave action density spectrum $N(\sigma, \theta)$, defined as the energy density spectrum divided by the relative frequency σ as observed in a reference frame moving with the current velocity, and with θ being the angle of wave incidence. The spectral wave action balance equation is given by:

$$\frac{\partial N}{\partial t} + \frac{\partial C_x N}{\partial x} + \frac{\partial C_y N}{\partial y} + \frac{\partial C_\sigma N}{\partial \sigma} + \frac{\partial C_\theta N}{\partial \theta} = \frac{S}{\sigma}, \quad (1)$$

with C_x, C_y, C_σ and C_θ the propagation velocities in x-, y-, σ- and θ-space, respectively, and t is time. $S(\sigma,\theta)$ is the sink term, representing the effects of depth-induced breaking and bottom friction dissipation and nonlinear wave–wave interactions as functions of frequency and direction. Default parameter set-

tings and time-invariant offshore wave forcing were used throughout this study.

The flow model is based on the time-averaged and depth-integrated mass and momentum conservation equations. The averaging duration is chosen to be much longer than the wave groups, but significantly shorter than any time-scale associated with changes in incident wave conditions. The hydrodynamics are solved using an implicit method to obtain quasi-steady mean water depth h and water volume fluxes Q_i, with the subscript i referring to the two horizontal coordinates:

$$\frac{\partial Q_i}{\partial t} + \frac{\partial}{\partial x_j}\left(\frac{Q_i Q_j}{h}\right) - gh\frac{\partial \eta}{\partial x_i} - \frac{1}{\rho}\frac{\partial S_{ij}}{\partial x_j} + \frac{1}{\rho}\frac{\partial T_{ij}}{\partial x_j} - \frac{T_i^{\text{b}}}{\rho}, \quad (2)$$

$$\frac{\partial \eta}{\partial t} + \frac{\partial Q_j}{\partial x_j} = 0. \quad (3)$$

In Equations (2) and (3), η is the mean free surface elevation, g the gravitational acceleration, ρ the water density, S_{ij} the radiation stress components (Philipps, 1977). With the mean horizontal current velocities given by $U_i = Q_i/h$ following Mei (1989), the bed shear stress τ_i^b according to the weak flow approximation (Liu and Dalrymple, 1978) is given by:

$$\tau_i^{\text{b}} = \rho C_f U_w U_i, \quad (4)$$

with U_w the near-bottom orbital velocity and C_f a spatially constant bottom friction coefficient. T_{ij} is the lateral shear stress which is the horizontal momentum exchange due to the combined action of turbulence and the mean current, using the formulation proposed by Battjes (1975):

$$T_{ij} = \rho h\left[Mh\left(\frac{D}{\rho}\right)^{1/3} + v_0\right]\left(\frac{\partial U_i}{\partial x_j} + \frac{\partial U_j}{\partial x_i}\right), \quad (5)$$

where D is the rate of energy loss due to depth-induced breaking, and M and v_0 are constants.

The bed and suspended load sediment transport $\vec{Q}_s$ was computed using the formulations of Bailard (1981), using default settings. The new seabed level Z_f was computed using the sediment mass conservation equation:

$$\frac{\partial Z_f}{\partial t} + \frac{1}{1-p}\vec{\nabla}\vec{Q}_s = 0, \quad (6)$$

where $p = 0\cdot4$ is the sediment porosity. The morphological time step for the bed update scheme was 1 hour throughout.

All the simulations were run with time-invariant mean water level (no tide). Our model does not include descriptions of the undertow, wave nonlinearity, wave–current interaction and surface rollers to limit model complexity; yet it still contains the essential physics to examine the initial growth and subsequent nonlinear evolution of crescentic patterns in double sandbar systems (Castelle and Bonneton, 2004; Castelle et al., 2006).

Initial bathymetries and grid

We ran the model for different double sandbar geometries on a computational grid with an alongshore length of 4200 m, 20×20 m grid cells, and periodic lateral boundary conditions. In each geometry, we implemented an alongshore-uniform inner bar, 100 m from the mean-sea-level shoreline and with its crest in 1 m water depth. Detailed bathymetric

Copyright © 2010 John Wiley & Sons, Ltd.

Earth Surf. Process. Landforms, Vol. **35**, 476–486 (2010)
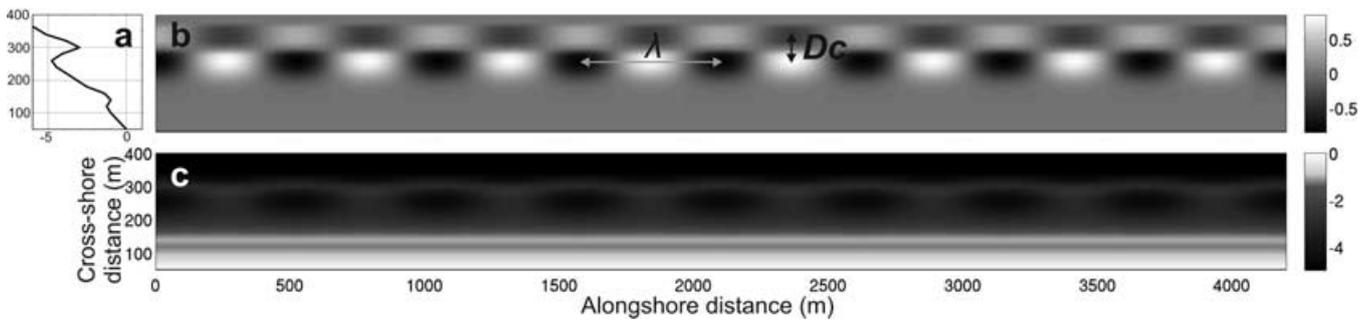
Figure 3. Example of an initial double sandbar geometry used for the simulations with (a) an alongshore-uniform double-barred beach profile with (b) a superimposed horn and bay sequence resulting in (c) outer-bar crescentic patterns, here with $\lambda = 525$ m, $D_c = 60$ m and $D_v = 1\cdot7$ m.
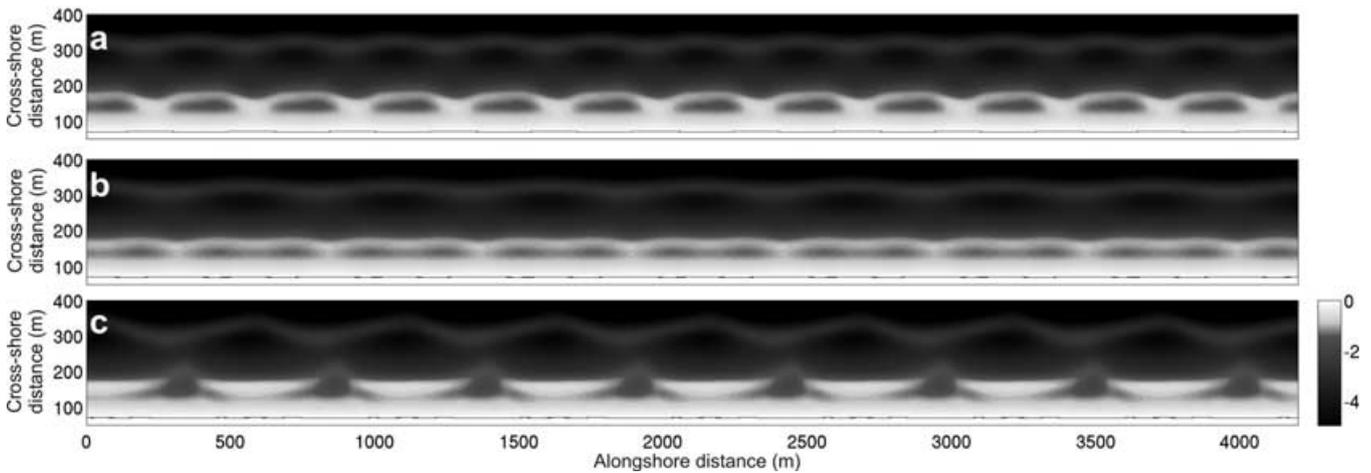
Figure 4. Simulated bathymetry for (a) initially outer-bar crescents with $\lambda = 350$ m, $D_c = 60$ m and $D_v = 1\cdot35$ m and constant wave forcing with $H_{s0} = 0\cdot8$ m after 7 days, (b) initially outer-bar crescents with $\lambda = 525$ m, $D_c = 60$ m and $D_v = 1\cdot7$ m and constant wave forcing with $H_{s0} = 0\cdot8$ m after 7 days, and (c) initially outer-bar crescents with $\lambda = 525$ m, $D_c = 60$ m and $D_v = 1\cdot7$ m and constant wave forcing with $H_{s0} = 1\cdot2$ m after 3 days. Simulated inner- and outer-bar relationship are (a) an in-phase coupling (inner-bar horns facing outer-bar horns), (b) coupling at half of the outer-bar wavelength and (c) 180° out-of-phase coupling (inner-bar horns facing outer-bar bays). The key indicates seabed elevation in metres (light is shallow, dark is deep).

surveys of crescentic bars are scarce. Therefore, the outer-bar geometries were loosely based on existing observations (e.g. Ruessink et al., 2007) but are still considered to be realistic. The outer bar was located 250 m from the mean-sea-level shoreline with its crest in 3 m water depth. Crescentic patterns were superimposed to the alongshore-uniform outer bar as an alongshore sequence of horns and bays alternating shoreward and seaward of the outer-bar crest. Three main parameters were used to characterize the crescentic bar geometry: the alongshore wavelength λ, the cross-shore amplitude between a horn and a bay D_c and the vertical amplitude of the bay/horn sequence D_v (Figure 3). The bars were superimposed on a 1 : 50 planar sloping depth profile, with its offshore extent in 10·5 m water depth.
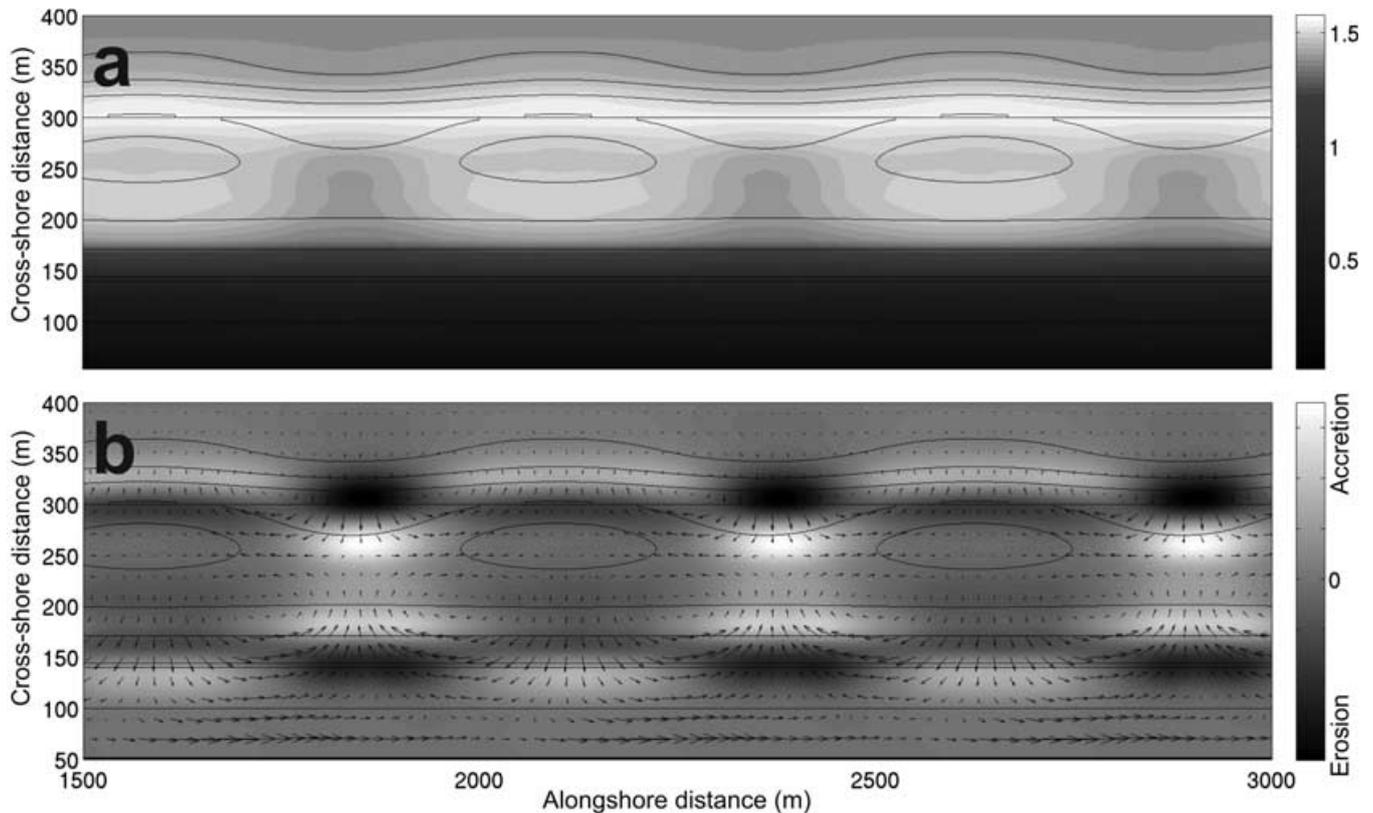
Results

Preliminary simulations suggested that D_c does not play a significant role in the simulated coupling patterns except, not surprisingly, for $D_c = 0$ which does not result in coupling patterns. The range of D_c values is strongly limited by the 20 m grid resolution. We set D_c to 60 m for all the initial outer-bar geometries. As the emergence of coupling patterns is favoured by small offshore wave angles with respect to shore normal, only shore-normal waves are considered. To further restrict the number of parameters and the complexity of the sensitivity

analysis, we considered shore-normal waves with an offshore peak period T_{p0} of 8 s. In total, 208 simulations were run to investigate the sensitivity of emerging coupling patterns to variations in λ, D_v and H_{s0} only. In our model there is no bed diffusion or bedslope transport (Garnier et al., 2008) likely to damp the instabilities. Continuing the simulations over a long duration would make the bed slope locally too large and the hydrodynamic model would eventually blow up. Accordingly, all the morphological evolutions presented below do not represent a steady state of the double sandbar system and are taken about 1–2 days before the sandbar morphologies become unrealistic.

Figure 4 shows examples of the three main coupling patterns simulated in this study: in-phase coupling (Figure 4a), with inner-bar horns facing outer-bar horns; coupling at half of the outer-bar wavelength (Figure 4b) with two inner-bar rip channels for one outer-bar crescent; 180° out-of-phase coupling (Figure 4c), with inner-bar bays facing outer-bar horns. Figure 5 displays the emerging coupling patterns as a function of λ, D_v and H_{s0}. It is to be noted that, in some simulations, coupling at half of the outer-bar wavelength initially emerges and eventually transforms into an in-phase coupling (which is indicated in Figure 5). This illustrates the strong nonlinear behaviour of the inner-bar dynamics. Results show that in-phase coupling is favoured by low-energy waves (Figures 5a, c), short outer-bar alongshore wavelengths (Figures 5a, c) and small vertical amplitudes of the outer-bar horn/bay sequence
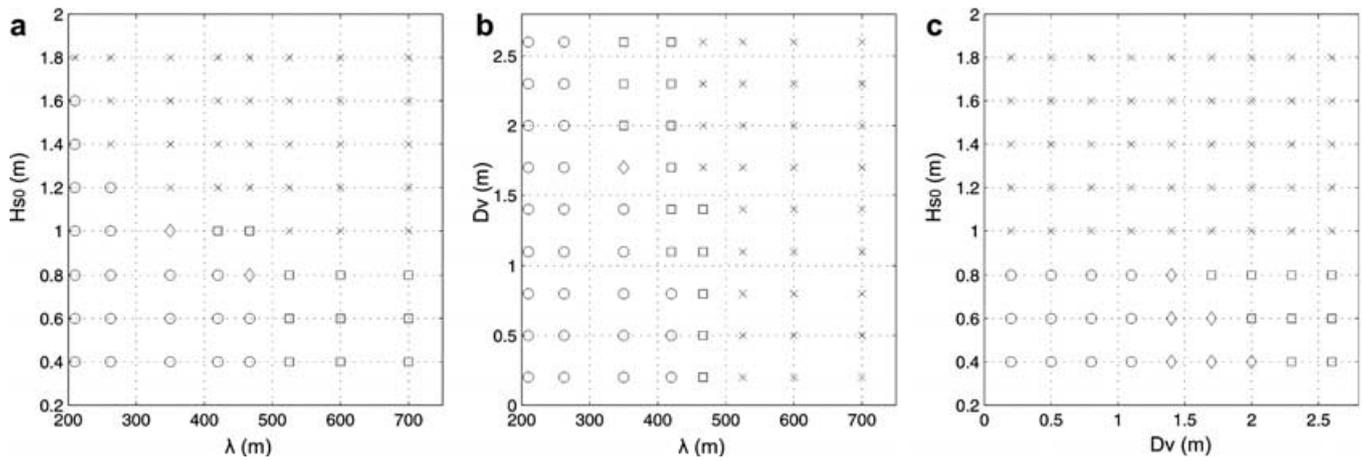
Figure 5. Emerging coupling pattern simulated by the nonlinear morphodynamic model as a function of (a) H_{s0} versus λ for $D_v = 1.7$ m, (b) D_v versus λ with $H_{s0} = 1$ m and (c) H_{s0} versus D_v with $\lambda = 525$ m. The circles indicate an in-phase coupling (Figure 4a), the squares a coupling at half of the outer-bar wavelength (Figure 4b), the crosses a 180° out-of-phase coupling (Figure 4c), and the diamonds a coupling at half of the outer-bar wavelength that eventually transforms into an in-phase coupling.
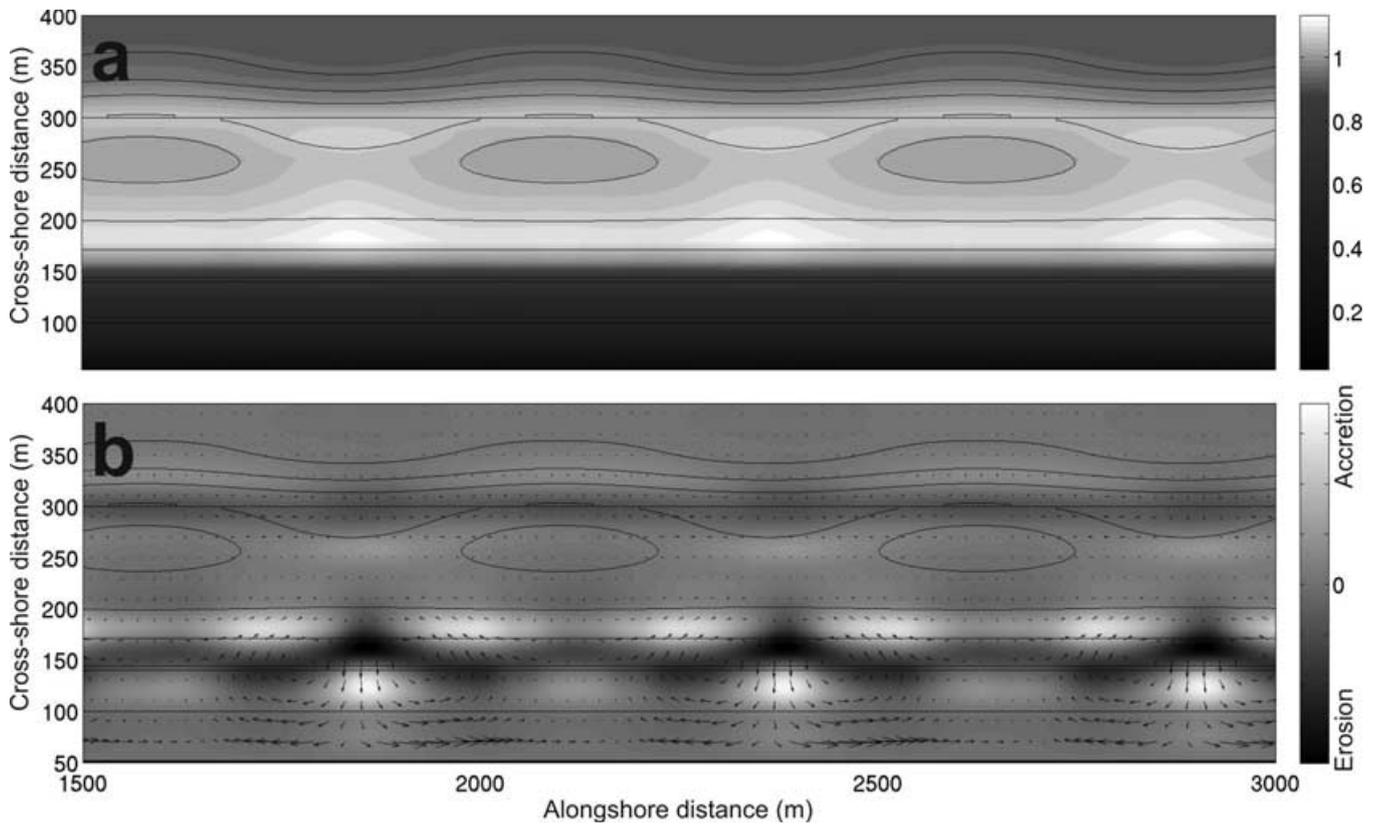

Figure 6. Simulation at $t = 0$ of (a) significant wave height and (b) resulting wave-induced current (maximum flow velocities reach 0·085 m s^{-1}) and erosion/accretion patterns for outer-bar crescents with $\lambda = 525$ m, $D_c = 60$ m and $D_v = 1.7$ m and constant offshore wave forcing with $H_{s0} = 1.2$ m; these settings lead to a 180° out-of-phase coupling (Figure 4c).

(Figures 5b, 5c). Slight increases in H_{s0}, λ or D_v favour a shifting from an in-phase coupling to a coupling at half of the outer-bar wavelength (Figure 5). For larger H_{s0}, λ or D_v, 180° out-of-phase coupling is observed. In other words, in-phase (180° out of phase) coupling can be observed for low (high) energy waves and weakly (well-) developed outer bars with crescentic patterns at small (large) alongshore wavelengths, where coupling at half of the outer-bar wavelength acts as an intermediate (variation of the in-phase) coupling pattern.

A more in-depth investigation of the hydrodynamics shows that wave refraction and depth-induced breaking patterns over the outer bar drive the initial development of coupling pat-

terns. The resulting shoreward variations in wave energy enforce alongshore variations in wave set-up which drive horizontal circulation patterns over the inner bar. Therefore, these inshore horizontal circulation patterns, and resulting initial erosion/accretion patterns, are linked to the more seaward outer-bar geometry.

The degree of wave breaking across the outer bar strongly influences the type of emerging coupling. This is especially true for the distinction between 180° out-of-phase coupling and the two other coupling patterns. Figure 6 shows the initial wave, flow and resulting erosion/accretion patterns leading to the 180° out-of-phase coupling shown in Figure 4c after three

Figure 7. Simulation at $t = 0$ of (a) significant wave height and (b) resulting wave-induced current (maximum flow velocities reach 0·075 m s^{-1}) and erosion/accretion patterns for outer-bar crescents with $\lambda = 525$ m, $D_c = 60$ m and $D_v = 1·7$ m and constant offshore wave forcing with $H_{s0} = 0·8$ m; these settings lead to a coupling at half of the outer-bar wavelength (Figure 4b).

days of simulations, with wave conditions of $H_{s0} = 1·2$ m and $T_{p0} = 8$ s and an outer-bar geometry with $\lambda = 525$ m, $D_c = 60$ m and $D_v = 1·7$ m. In this case, depth-induced wave breaking is observed over the outer-bar horns, which results in lower wave energy shoreward of each horn (Figure 6a). The resulting alongshore patterns in wave set-up drives horizontal circulation patterns, with a single rip current over the inner bar (and a resulting erosion area) facing one outer-bar horn (Figure 6b). The temporal evolution of the morphology eventually leads to the 180° out-of-phase coupling observed in Figure 4c. In contrast, with lower offshore wave energy ($H_{s0} = 0·8$ m, $T_{p0} = 8$ s) and a similar outer-bar geometry, there is no wave breaking across the outer bar but only refraction which results in wave energy focusing shoreward of the outer-bar horn (Figure 7a). This induces an onshore flow over the inner bar facing an outer-bar horn (Figure 7b). In this case (an outer-bar wavelength λ of 525 m), the distance between each inner-bar onshore flow is large enough for two offshore flows (rip currents) to form for one outer-bar crescent, resulting in two distinct erosion areas over the inner bar (Figure 7b). The temporal evolution of the morphology eventually leads to the coupling patterns at half of the outer-bar wavelength observed in Figure 4b. For shorter outer-bar wavelength and similar D_v and D_c, for instance with $\lambda = 350$ m, the distance between the two onshore flows is too small to drive two sufficiently distinct offshore-directed flows. In this case, the inner-bar morphology, through the positive feedback between hydrodynamics, sediment transport and the evolving morphology, develops a single rip channel facing an outer-bar bay and, eventually, leads to the in-phase coupling observed in Figure 4a, with the two onshore flows only feeding one confined rip current system.

The impact of the degree of wave breaking across the outer bar on the coupling patterns can be assessed in more detail in Figure 8 (for which additional simulations have been made, with H_{s0} values every 0·05 m), here in the case of initial outer bar with $\lambda = 525$ m, $D_c = 60$ m and $D_v = 1·7$ m. Results show that change from wave breaking across the outer bar to non-breaking drastically controls alongshore variations of the wave height and resulting onshore and offshore flow patterns along the inner-bar crest. More importantly, this shows that all the shore-normal waves with H_{s0} above a threshold value delimiting wave breaking and non-breaking across the outer bar (in this case 0·95 m), will favour the 180° out-of-phase coupling shown in Figure 4c. Similarly, all the shore-normal waves with H_{s0} below the threshold value will favour the coupling at half of the outer-bar wavelength shown in Figure 4c.

This threshold value of $H_{s0} = 0·95$ m is true for outer bars with large wavelengths ($\lambda > 480$ m, Figure 5a). This change in coupling pattern takes place at different H_{s0} values for smaller wavelengths (Figure 5a), which suggests a more complicated process than the onset of wave breaking alone. For smaller outer-bar wavelengths, wave focusing by refraction is more important than for larger outer-bar wavelengths, and the relative importance of wave breaking across the outer bar and wave focusing controls the change in coupling pattern. Figure 9 shows examples of the relative importance of wave breaking and wave focusing by refraction. For an initial outer bar with $\lambda = 525$ m, $D_c = 60$ m and $D_v = 1·7$ m (Figure 9a) and for $H_{s0} = 0·8$ m, larger waves are observed shoreward of each outer-bar horn (Figure 9b) as the fraction of breaking waves Q_b across the outer bar is not significant (Figure 9c), resulting in the emergence of coupling at half of the outer-bar

Copyright © 2010 John Wiley & Sons, Ltd.

Earth Surf. Process. Landforms, Vol. 35, 476–486 (2010)
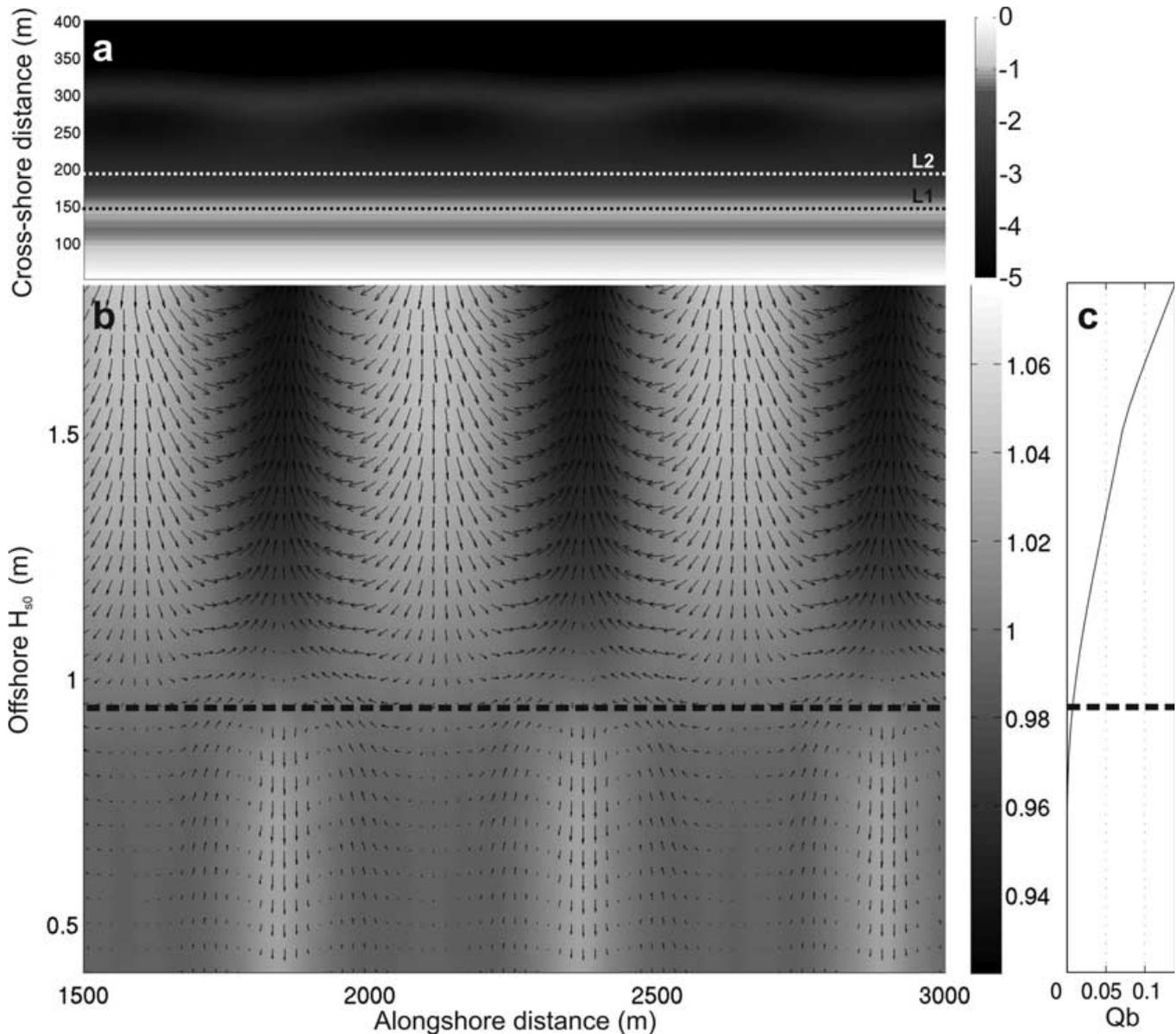
Figure 8. (a) Initial outer bar with $\lambda = 525$ m, $D_c = 60$ m and $D_v = 1\cdot7$ m and (b) $H_{s2}/\overline{H_{s2}}$, with H_{s2} denoting the significant wave height H_s along the alongshore line *L2* located immediately seaward of the inner bar and $\overline{H_{s2}}$ the alongshore average of H_{s2}, versus offshore significant wave height H_{s0}, with superimposed wave-induced currents vectors $\vec{U_1}$ along the alongshore line *L1* over the bar crest; the dark dashed line in (b) indicates the limit between depth-induced breaking and non-breaking across the outer bar as indicated by (c) the computed fraction of breaking waves Q_b as a function of H_{s0}.

wavelength (Figure 5a). Increasing H_{s0} to 1 m leads to a Q_b of about 0·01 across the outer-bar horns (Figure 9c) which is small but sufficient to overwhelm wave focusing by refraction, resulting in smaller waves shoreward of each outer-bar horn (Figure 5b) and the emergence of a 180° out-of-phase coupling (Figure 5a). For an outer bar with $\lambda = 210$ m (Figure 9d) and for $H_{s0} = 1\cdot2$ m, larger Q_b of about 0·035 are computed across the outer-bar horn (Figure 9f). This fraction of breaking wave is not sufficient to overwhelm wave focusing by refraction (Figure 9e) resulting in the emergence of coupling at half of the outer-bar wavelength (Figure 5a). Larger Q_b values are now required for wave breaking to overwhelm wave focusing by refraction. In the case of an outer bar with $\lambda = 210$ m, the overwhelming of wave focusing by wave breaking is observed for $Q_b > 0\cdot09$ (Figure 9f), that is for $H_{s0} > 1\cdot7$ m, which results in the emergence of 180° out-of-phase coupling (Figure 5a).

Discussion and Conclusions

Our simulations show that coupling patterns arise from horizontal circulation patterns driven by alongshore variations in wave set-up enforced by wave refraction and depth-induced breaking over the outer bar. The relative importance of wave focusing by refraction versus wave breaking across the outer bar controls the inner-bar patterns morphologically forced by the outer bar. For large λ, wave focusing is relatively unimportant and is overwhelmed by wave breaking once waves start to break across the outer bar. For smaller λ, wave focusing by refraction is much more important and a larger fraction of breaking waves across the outer bar is required for overwhelming wave focusing. When wave breaking overwhelms wave focusing, 180° out-of-phase coupling emerges regardless of the outer-bar wavelength. When wave focusing by refraction overwhelms wave breaking, coupling at half of the
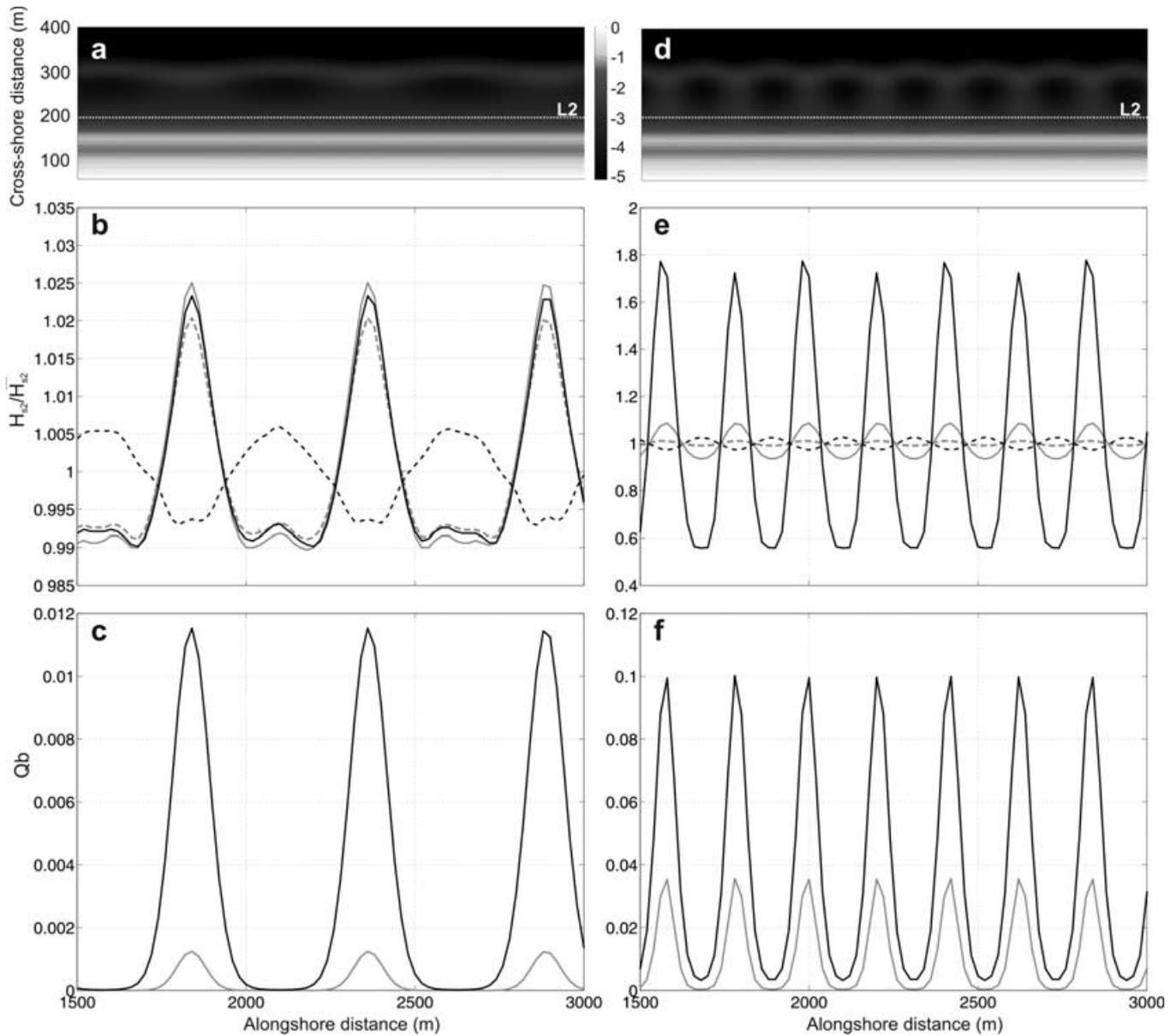
Figure 9. (a) Initial outer bar with $\lambda = 525$ m, $D_c = 60$ m and $D_v = 1 \cdot 7$ m, (b) $H_{s2}/\overline{H_{s2}}$, with H_{s2} denoting the significant wave height H_s along the alongshore line *L2* with deactivated wave breaking (wave refraction alone, solid line) and with wave breaking (dotted line) and (c) fraction of breaking waves along the outer bar, for $H_{s0} = 0 \cdot 8$ m and 1 m in grey and black, respectively; (d) Initial outer bar with $\lambda = 210$ m, $D_c = 60$ m and $D_v = 1 \cdot 7$ m, (e) $H_{s2}/\overline{H_{s2}}$ with deactivated wave breaking (wave refraction alone, solid line) and with wave breaking (dotted line) and (f) fraction of breaking waves along the outer bar, for $H_{s0} = 1 \cdot 2$ m and $1 \cdot 7$ m in grey and black, respectively.

outer-bar wavelength (in phase) is observed for larger (smaller) outer-bar wavelength and larger (smaller) vertical amplitude of the horn and bay sequence.

The simulated 180° out-of-phase coupling patterns are essentially similar to the observations of Van Enckevort and Wijnberg (1999) and Castelle *et al.* (2007) on two contrasting wave-dominated multiple-barred beaches. Figure 10 shows an example of a qualitative comparison of simulated patterns with observations. In the case of no wave breaking across the outer bar, two other coupling patterns can arise. For weakly developed crescents with short alongshore wavelengths and low-energy waves, an in-phase coupling is observed with inner-bar horns facing outer-bar horns. Despite no evidence of such a coupling pattern in double sandbar systems being found in the literature, this coupling can be considered as reminiscent of the more commonly observed in-phase relationship between inner-bar patterns and shoreline rhythms

(Figure 2b). When increasing the outer-bar alongshore wavelength, the vertical amplitude of the horn/bay sequence or the offshore wave height (maintaining non-breaking condition across the outer bar), coupling at half of the outer-bar wavelength is observed with the systematic occurrence of two inner-bar rip channels for one outer-bar crescent. Field observations of these simulated coupling patterns (Castelle *et al.*, 2007; also Figures 1 and 11) enforce the confidence we can have in the numerical results and the underlying mechanisms responsible for the emergence of coupling. In the field, the rapid time-varying offshore wave conditions with respect to the slower morphological time response of surfzone sandbars would suggest that such striking coupling patterns can hardly form. In addition, variations in mean water depth induced by tides continuously change the balance between wave breaking and refraction across the outer bar, which was not taken into account in our model. Despite being readily

Copyright © 2010 John Wiley & Sons, Ltd.

Earth Surf. Process. Landforms, Vol. **35**, 476–486 (2010)
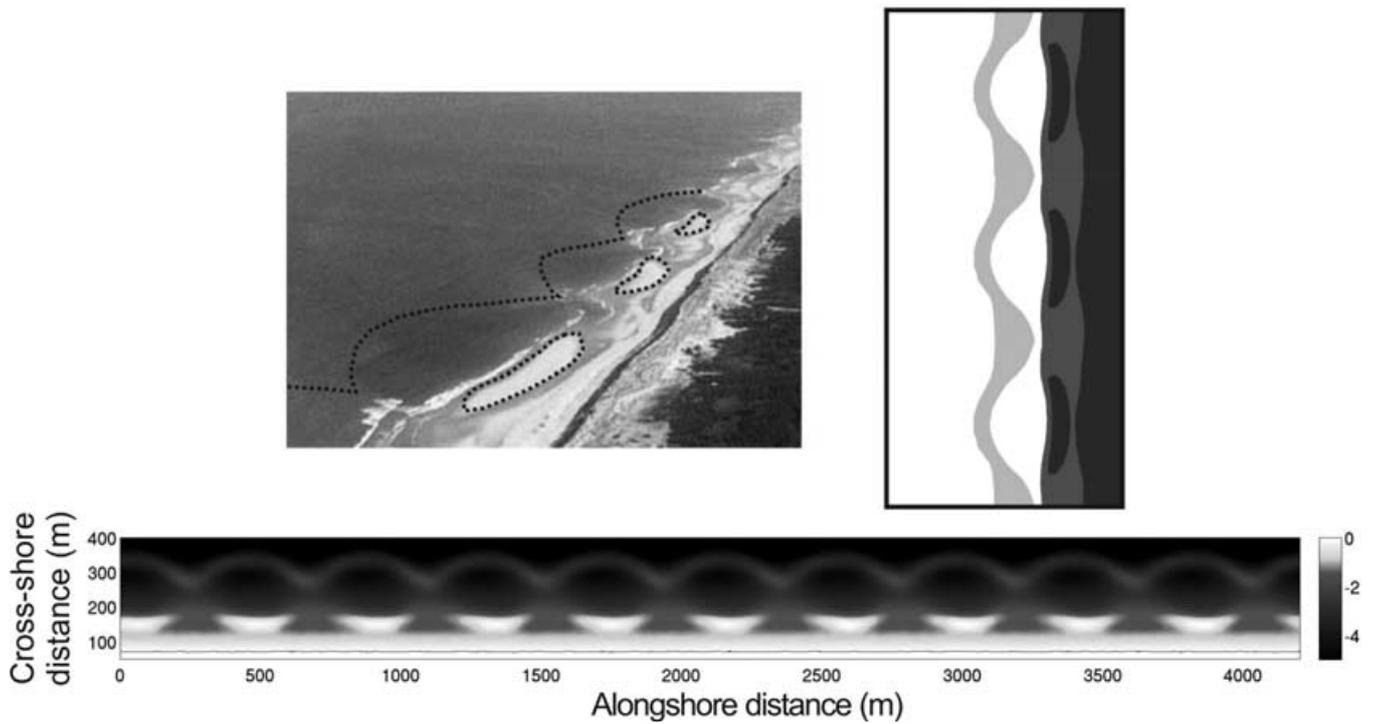
Figure 10. Computed 180° out-of-phase coupling patterns with an outer-bar horn facing an inner-bar bay, favoured in the presence of high-energy shore-normal waves, similar to some observations on a meso- macro-tidal high-energy double-barred beach in Castelle *et al.* (2007).
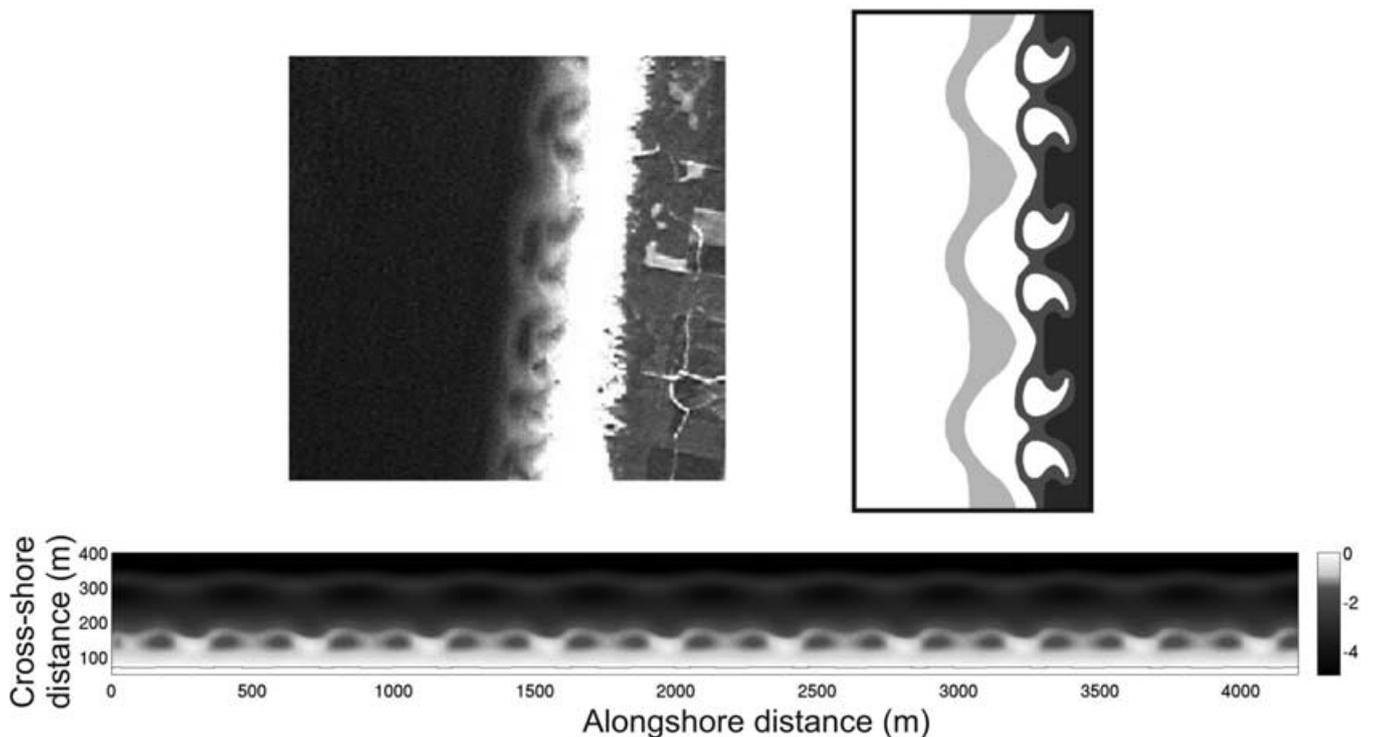
Figure 11. Computed coupling patterns at half of the outer-bar wavelength, favoured in the presence of low-energy shore-normal waves and large outer-bar wavelength, similar to some observations on a meso- macro-tidal high-energy double-barred beach in Castelle *et al.* (2007).

apparent in Figures 10 and 11, emergence of coupling patterns in meso- to macro-tidal environments is potentially more complicated than in the idealized simulations presented in this paper. Further simulations with tides will be required to examine the effects of mean water level variations on the (intertidal) inner-bar dynamics.

Coco and Murray (2007) reviewed the sweeping shift from forcing template to self-organization for explaining the forma-tion of rhythmic surfzone sandbars, among other nearshore patterns. Morphological coupling does not appear to fit in this classification. On the one hand, the inshore horizontal circu-lation patterns and resulting inner-bar rip channel develop-ment are forced by the more seaward outer-bar geometry through wave refraction and wave breaking across the outer bar. Morphological coupling implies the presence of a template in the morphology (outer-bar geometry) which,

Copyright © 2010 John Wiley & Sons, Ltd.

Earth Surf. Process. Landforms, Vol. **35**, 476–486 (2010)

therefore, can be seen as a forcing template. On the other hand, the inner-bar rip channels simulated herein with the nonlinear morphodynamic model also form through the positive feedback between hydrodynamics (waves and currents), sediment processes and the evolving bathymetry. In this case, the inner-bar morphology does not passively respond to the template in the hydrodynamics enforced by the outer-bar geometry. Morphological coupling, therefore, can also be seen as self-organization. In the case of sufficient offshore wave energy, the outer bar also evolves significantly (Figure 4c), which means that the forcing template in the morphology is time-varying and governed by self-organization mechanisms. Eventually, the outer-bar horns weld to the inner bar and sections of the forcing template become part of the morphologically forced inner bar.

Morphological coupling can thus be seen as a novel mechanism that blurs the distinction between forcing template and self-organization mechanisms. This mechanism may also be extended to explain the dynamics of other striking morphological patterns exhibited in the nearshore region. For instance, Holland and Holman (1996) observed the formation of shorter-scale cusps with spacings of approximately half that of the most well-developed cusps located at a higher beach level. The authors suggested that a slight change in tidal level or incident wave period might have induced resonantly forced edge waves which, in turn, forced the formation of cusps at half of the larger cusp wavelength. This edge-wave forced response of the smaller beach cusps is not consistent with the recent abandonment of the forcing template explanation. Despite the obvious differences between surfzone sandbar and beach cusp dynamics (beach cusps form in the swash zone, nearshore bars form in the surf zone), the formation of these smaller cusps at half of the larger cusp wavelength may actually be formed through swash zone coupling mechanisms analogous to the surfzone morphological coupling mechanism presented in this paper. In this case, the morphological response of the lower cusps, following a slight decrease in tidal level or a change in incident wave conditions, may be morphologically forced by the higher, larger cusps. This hypothesis cannot be tested with the kind of nonlinear morphodynamic model used in this study and has to be explored further with self-organization models based on swash zone processes (Werner and Fink, 1993; Coco et al., 2004). In addition, our study shows that coupling in double sandbar systems can be considered as reminiscent of the commonly observed relationship between inner-bar patterns and shoreline rhythms. Similarly, sandbar coupling with seaward sorted bedforms (nearshore geological features, i.e. morphological template) may exist, reminiscent of their observed relationship with shoreline undulations (Browder and McNinch, 2006; Schupp et al., 2006). This morphodynamic coupling between other morphological patterns needs to be explored further.

Our numerical model successfully simulated coupling patterns in double sandbar systems observed in the field, and allowed the description of a novel mechanism likely to play an important role in surfzone sandbar dynamics, and for other nearshore patterns. Clear coupling patterns in double sandbar systems, such as in Figures 1, 8 and 9, are however rarely observed in the field (Van Enckevort and Wijnberg, 1999; Castelle et al., 2007; Quartel, 2009). More often, inner-bar rip channels possess remarkably smaller and more variable alongshore scales than the outer bar (e.g. Barusseau et al., 1994; Van Enckevort et al., 2004; Lafon et al., 2004, 2005). This would suggest that morphological coupling does not play a substantial role in the overall double-sandbar dynamics. However, additional simulations with our numerical model show that this variability actually arises from a mixture of morphological coupling and self-organization mechanisms. The general field observation that inner-bar rip channels are more irregularly spaced than outer-bar crescents suggests that morphological coupling may be more important to understanding and predicting the evolution of inner-bar rip channels than previously envisaged. This issue is explored in the companion paper (Castelle et al., 2010).

References

Ashton A, Murray AB, Arnault O. 2001. Formation of coastline features by large-scale instabilities induced by high-angle waves. *Nature* **414**: 296–300.

Bailard JA. 1981. An energetics total load sediment transport model for a plane beach. *Journal of Geophysical Research* **86**: C11, 10938–10954.

Barusseau J-P, Radulescu M, Descamps C, Akouango E, Gerbe A. 1994. Morphosedimentary multiyear changes on a barred coast (Gulf of Lions, Mediterranean Sea, France). *Marine Geology* **122**: 47–62.

Battjes JA. 1975. Modelling of turbulence in the surfzone. In *Proc. Symposium on Modelling Techniques* ASCE: New York. 1050–1061.

Booij N, Ris RC, Holthuijsen LH. 1999. A third-generation wave model for coastal regions, Part 1: Model description and validation. *Journal of Geophysical Research* **104**: C4, 7649–7666.

Bowen AJ. 1997. Patterns in the water: Patterns in the sand? In *Proceedings of Coastal Dynamics '97* ASCE: New York. 1–10.

Bowen AJ, Inman DL. 1971. Edge waves and crescentic bars. *Journal of Geophysical Research* **76**: 8662–8671.

Bowman D, Goldsmith V. 1983. Bar morphology of dissipative beaches: an empirical model. *Marine Geology* **51**: 15–33.

Browder AG, McNinch JE. 2006. Linking framework geology and nearshore morphology: correlation of paleo-channels with shore-oblique sandbars and gravel outcrops. *Marine Geology* **231**: 141–162.

Bryan KR, Bowen AJ. 1997. Can bar-trapped edge waves cause bar formation, bar movement or bar growth? In *Proceedings of the 13th Australasian Coastal and Ocean Engineering Conference and the 6th Australasian Port and Harbour Conference* **2**: 1037–1042.

Caballeria M, Coco G, Falqués A, Huntley DA. 2002. Self-organization mechanisms for the formation of nearshore crescentic and transverse bars. Journal of Fluid Mechanics **465**: 379–410.

Calvete D, Dodd N, Falqués A, Van Leeuwen SM. 2005. Morphological development of rip channel systems: Normal and near-normal wave incidence. *Journal of Geophysical Research* **110**: C10006, DOI: 10.1029/2004JC002803.

Carter RWG. 1988. *Coastal Environments* Academic Press:

Carter TG, Liu PL, Mei CC. 1973. Mass transport by waves and offshore bedforms. *Journal of the Waterways, Harbors and Coastal Engineering Division* **99**: 165–184. London, UK.

Castelle B, Bonneton P. 2004. Nearshore waves and currents over crescentic bars. *Journal of Coastal Research* S.I. 39, 687–691.

Castelle B, Bonneton P, Butel R. 2006. Modeling of crescentic pattern development of nearshore bars: Aquitanian Coast, France. *C. R. Geoscience* **338**: 795–801.

Castelle B, Bonneton P, Dupuis H, Sénéchal N. 2007. Double bar beach dynamics on the high-energy meso-macrotidal French Aquitanian Coast: A review. *Marine Geology* **245**: 141–159.

Castelle B, Ruessink BG, Bonneton P, Marieu V, Bruneau N, Price TD. 2010. Coupling mechanisms in double sandbar systems. Part 2: Impact on alongshore variability of inner-bar rip channels. *Earth Surface Processes and Landforms* DOI: 10.1002.esp.1949.

Clarke LB, Wermer BT. 2004. Tidally modulated occurrence of megar-ipples in a saturated surf zone. *Journal of Geophysical Research* **109**: C1012, DOI: 10.1029/2003JC001934.

Coco G, Murray AB. 2007. Patterns in the sand: from forcing templates to self-organization. *Geomorphology* **91**: 271–290.

Coco G, O'Hare TJ, Huntley DA. 1999. Beach cusps: a comparison of data and theories for their formation. *Journal of Coastal Research* **15**: 741–749.

Coco G, Burnet TK, Werner BT, Elgar S. 2004. The role of tides in beach cusp development. *Journal of Geophysical Research* **109**: C04011, DOI: 10.1029/2003JC002154.

Coco G, Bryan KR, Green MO, Ruessink BG, Turner IL. 2005. Video observations of shoreline and sandbar coupled dynamics. In *Proceedings of Coasts and Ports 2005* 471–476.

Damgaard J, Dodd N, Hall L, Chesher T. 2002. Morphodynamic modeling of rip channel growth. *Coastal Engineering* **43**: 199–221.

Deigaard R, Drønen N, Fredsøe J, Jensen JH, Jørgensen MP. 1999. A morphological stability analysis for a long straight barred coast. *Coastal Engineering* **36**: 171–195.

Drønen N, Deigaard R. 2007. Quasi-three-dimensional modelling of the morphology of longshore bars. *Coastal Engineering* **54**: 197–215.

Falqués A, Coco G, Huntley DA. 2000. A mechanism for the generation of wave-driven rhythmic patterns in the surf zone. *Journal of Geophysical Research* **105**: 24071–24088.

Gallagher EL, Elgar S, Thornton EB. 1998. Observations and predictions of megaripple migration in a natural surf zone. *Nature* **394**: 165–168.

Garnier R, Calvete D, Falqués A, Dodd N. 2008. Modelling the formation and the long-term behavior of rip channel systems from the deformation of a longshore bar. *Journal of Geophysical Research* **113**: C07053, DOI: 10.1029/2007JC004632.

Goldsmith V, Bowman D, Kiley K. 1982. Sequential stage development of crescentic bars: HaHoterim Beach, Southeastern Mediterranean. *Journal of Sedimentary Petrology* **52**: 233–249.

Greenwood B, Davidson-Arnott RGD. 1979. Sedimentation and equilibrium in wave-formed bars: A review and case study. *Canadian Journal of Earth Sciences* **16**: 312–332.

Guza RT, Inman DL. 1975. Edge waves and beach cusps. *Journal of Geophysical Research* **80**: 21, 2997–3012.

Holland KT, Holman RA. 1996. Field observations of beach cusps and swash motions. *Marine Geology* **134**: 77–93.

Holman RA. 2000. Pattern formation in the nearshore. In *Proceedings of River, Coastal and Estuarine Morphodynamics* Springer-Verlag: New York. 141–162.

Holman RA, Bowen AJ. 1982. Bars, bumps and holes: Models for the generation of complex beach topography. *Journal of Geophysical Research* **87**: 457–468.

Holman RA, Symonds G, Thornton EB, Ranasinghe R. 2006. Rip spacing and persistence on an embayed beach. *Journal of Geophysical Research* **111**: C06006, DOI: 10.1029/2005JC002965.

Hom-ma M, Sonu C. 1962. Rhythmic pattern of longshore bars related to sediment characteristics. In *Proceedings of 8th Internat. Conference on Coastal Engineering* ASCE: New York. 248–278.

Klein MD, Schuttelaars HM. 2006. Morphodynamic evolution of double-barred beaches. *Journal of Geophysical Research* **111**: C06017, DOI: 10.1029/2005JC003155.

Komar PD. 1998. *Beach processes and sedimentation*. Prentice Hall:

Lafon V, De Melo Apoluceno D, Dupuis H, Michel D, Howa H, Froidefond J-M. 2004. Morphodynamics of nearshore rhythmic sandbars in a mixed-energy environment (SW France): I. Mapping beach changes using visible satellite imagery. *Estuarine, Coastal and Shelf Science* **61**: 289–299.

Lafon V, Dupuis H, Butel R, Castelle B, Michel D, Howa H, De Melo Apoluceno D. 2005. Morphodynamics of nearshore rhythmic sandbars in a mixed-energy environment (SW France): II. Physical

forcing analysis. *Estuarine, Coastal and Shelf Science* **65**: 449–462.

Liu PL-F, Dalrymple RA. 1978. Bottom frictional stresses and longshore currents due to waves with large angles of incidence. *Journal of Marine Research* **36**: 357–375.

MacMahan JH, Thornton EB, Stanton TP, Reniers AJHM. 2005. RIPEX-observations of a rip current system. *Marine Geology* **218**: 113–134.

Marieu V, Bonneton P, Foster DL, Ardhuin F. 2008. Modeling of vortex ripple morphodynamics. *Journal of Geophysical Research* **113**: C09007, DOI: 10.1029/2007JC004659.

Mei CC. 1989. *Applied dynamics of ocean waves*. World Scientific: Singapore.

Philipps OM. 1977. *The dynamics of the upper ocean*. Cambridge University Press: Cambridge, UK.

Quartel S. 2009. Temporal and spatial behaviour of rip channels in a multiple-barred coastal system. *Earth Surface Processes and Landforms* **34**: 163–176.

Ranasinghe R, Symonds G, Black K, Holman R. 2004. Morphodynamics of intermediate beaches: A video imaging and numerical modelling study. *Coastal Engineering* **51**: 629–655.

Reniers AJHM, Roelvink JA, Thornton EB. 2004. Morphodynamic modeling of an embayed beach under wave group forcing. *Journal of Geophysical Research* **109**: C01030, DOI: 10.1029/2002JC001586.

Ruessink BG, Jeuken MCJL. 2002. Dunefoot dynamics along the Dutch coast. *Earth Surface Processes and Landforms* **27**: 1043–1056.

Ruessink BG, Coco G, Ranasinghe R, Turner IL. 2007. Coupled and noncoupled behavior of three-dimensional morphological patterns in a double sandbar system. *Journal of Geophysical Research* **112**: C07002, DOI: 10.1029/2006JC003799.

Schupp CA, McNinch JE, List JH. 2006. Nearshore shore-oblique bars, gravel outcrops, and their correlation to shoreline change. *Marine Geology* **233**: 63–79.

Shepard FP. 1952. Revised nomenclature for depositional coastal features. *Bulletin of the American Association of Petroleum Geology* **36**: 1902–1912.

Short AD. 1991. Macr-meso tidal beach morphodynamics – An overview. *Journal of Coastal Research* **7**: 2, 414–436.

Short AD. 1999. *Handbook of beach and shoreface morphodynamics*. Wiley: Chichester, UK.

Smit MWJ, Reniers AJHM, Ruessink BG, Roelvink JA. 2008. The morphological response of a nearshore double sandbar system to constant wave forcing. *Coastal Engineering* **55**: 761–770.

Sonu CJ. 1972. Field observation of nearshore circulation and meandering currents. *Journal of Geophysical Research* **77**: 18, 3232–3247.

Sonu CJ. 1973. Three-dimensional beach changes. *Journal of Geology* **81**: 42–64.

Thornton EB, MacMahan JH, Sallenger AH Jr. 2007. Rip currents, mega-cusps, and eroding dunes. *Marine Geology* **240**: 151–167.

Traykovski P, Hay AE, Irish JD, Lynch JF. 1999. Geometry, migration, and evolution of wave orbital ripples at LEO-A5. *Journal of Geophysical Research* **104**: C1, 1505–1524.

Van Enckevort IMJ, Wijnberg KM. 1999. Intra-annual changes in bar plan shape in a triple bar system. In *Proceedings of Coastal Sediments '99* 2548–2558.

Van Enckevort IMJ, Ruessink BG, Coco G, Suzuki K, Turner IL, Plant NG, Holman RA. 2004. Observations of nearshore crescentic sandbars. *Journal of Geophysical Research* **109**: C06028, DOI: 10.1029/2003JC002214.

Werner BT, Fink TM. 1993. Beach cusps as self-organised patterns. *Science* **260**: 968–971.

Wright LD, Short AD. 1984. Morphodynamic variability of surf zones and beaches: A synthesis. *Marine Geology* **56**: 93–118.